Removal of immunoglobulin-like domains from titin's spring segment alters titin splicing in mouse skeletal muscle and causes myopathy

Danielle Buck,[1,2] John E. Smith III,[1] Charles S. Chung,[1] Yasuko Ono,[3] Hiroyuki Sorimachi,[3] Siegfried Labeit,[4] and Henk L. Granzier[1]

[1]Department of Physiology and [2]Department of Molecular and Cellular Biology, University of Arizona, Tucson, AZ 85721
[3]Calpain Project, Tokyo Metropolitan Institute of Medical Science (IGAKUKEN), Setagaya-ku, Tokyo 156-8506, Japan
[4]Department of Integrative Pathophysiology, University Medical Centre Mannheim, University of Heidelberg,
 68167 Mannheim, Germany

Titin is a molecular spring that determines the passive stiffness of muscle cells. Changes in titin's stiffness occur in various myopathies, but whether these are a cause or an effect of the disease is unknown. We studied a novel mouse model in which titin's stiffness was slightly increased by deleting nine immunoglobulin (Ig)-like domains from titin's constitutively expressed proximal tandem Ig segment (IG KO). KO mice displayed mild kyphosis, a phenotype commonly associated with skeletal muscle myopathy. Slow muscles were atrophic with alterations in myosin isoform expression; functional studies in soleus muscle revealed a reduced specific twitch force. Exon expression analysis showed that KO mice underwent additional changes in titin splicing to yield smaller than expected titin isoforms that were much stiffer than expected. Additionally, splicing occurred in the PEVK region of titin, a finding confirmed at the protein level. The titin-binding protein *Ankrd1* was highly increased in the IG KO, but this did not play a role in generating small titin isoforms because titin expression was unaltered in IG KO mice crossed with *Ankrd1*-deficient mice. In contrast, the splicing factor RBM20 (RNA-binding motif 20) was also significantly increased in IG KO mice, and additional differential splicing was reversed in IG KO mice crossed with a mouse with reduced RBM20 activity. Thus, increasing titin's stiffness triggers pathological changes in skeletal muscle, with an important role played by RBM20.

INTRODUCTION

Titin, the largest known protein (3–4 MD), resides in the sarcomere of striated muscle, where it extends from the Z disk to the M band and is responsible for the intracellular passive stress that develops when muscle is stretched (Fürst et al., 1988; Linke et al., 1994; Ottenheijm and Granzier, 2010). Titin-based passive stress maintains the central position of the A band in the sarcomere (Horowits and Podolsky, 1987), which is important for efficient contraction, controls the physiological sarcomere length (SL) range (Granzier et al., 2009), and plays a role in various stress-dependent signaling pathways through its interaction with multiple binding partners (Fukuda et al., 2008; LeWinter and Granzier, 2010; Linke and Krüger, 2010; Gautel, 2011). Titin is encoded by a single gene, and differential splicing of the extensible spring-like segment of the titin molecule can vary the passive stress of muscles (Bang et al., 2001; Granzier and Labeit, 2007). The spring segment in skeletal muscle consists of the PEVK region (so named because it is rich in proline, glutamic acid, valine, and lysine residues) and the proximal and distal tandem Ig-like–containing segments, located near the Z disk and the A band, respectively (Labeit and Kolmerer, 1995; Bang et al., 2001; Fig. 1). Titin's serially linked Ig-like domains have a β-barrel fold characteristic of the intermediate I-set of the Ig superfamily (Pfuhl and Pastore, 1995); their linker sequences unbend upon sarcomere stretch, giving rise to an increased end to end length of the tandem Ig segments. Differential splicing of the PEVK and Ig-like regions leads to the production of a titin protein that varies in size depending on the species, muscle type, and developmental stage, with a decrease in size that is associated with an increase in passive stress in the sarcomere (Prado et al., 2005; Ottenheijm et al., 2009b). Advancement in our understanding of the contribution of these spring-like elements of titin to the generation of passive stress have been made through the generation of mouse models in which various portions of the spring have been deleted. These include the deletion of exon 49, which encodes the cardiac-specific N2B element (Radke et al., 2007), exons 219–225, which encode part of the PEVK region (Granzier et al., 2009), and exons 30–38, which encode 9 of the 15

Correspondence to Henk L. Granzier: granzier@email.arizona.edu

Abbreviations used in this paper: COPD, chronic obstructive pulmonary disorder; CSA, cross-sectional area; ECM, extracellular matrix; EDL, extensor digitorum longus; MHC, myosin heavy chain; RRM, RNA recognition motif; SL, sarcomere length; TC, tibialis cranialis.

constitutively expressed proximal tandem Ig domains (Chung et al., 2013). Such models have been used to study the effects of spring element deletion on the physiology of cardiac muscle, but an in-depth investigation of the role of titin in skeletal muscle has not been performed. This is an important area of research considering that passive stress is altered in various skeletal muscle myopathies (Ottenheijm et al., 2006, 2012; Ottenheijm and Granzier, 2010; van Hees et al., 2010, 2012); it is unknown to what extent changes in titin are an effect of the myopathy or can cause myopathic changes.

Here, we studied how skeletal muscle responds to deleting the constitutively expressed proximal Ig domains 3–11 (titin exons 30–38; mouse model referred to as IG KO) using a multidisciplinary approach that includes gene expression analysis, titin protein analysis, muscle mechanics, and mouse genetics. We found that in the IG KO mouse, skeletal muscle undergoes additional differential splicing to yield smaller titin isoforms, which results in greatly increased passive stress. Surprisingly, there are also changes in muscle trophicity and contractility. Exon expression analysis revealed that the small titin isoforms expressed in IG KO mice are full-length titins that arise through removal of PEVK sequences. We analyzed titin-binding proteins and found *Ankrd1* (also called CARP [cardiac ankyrin repeat protein] or MARP1 [muscle ankyrin repeat protein 1]) to be highly up-regulated, but by crossing the IG KO mouse with a mouse deficient in *Ankrd1*, we obtained conclusive evidence that *Ankrd1* is not necessary for additional titin

splicing to take place. We also determined the expression level of the recently discovered titin splicing factor RBM20 (RNA-binding motif protein 20; Guo et al., 2012) and found it to be up-regulated in IG KO soleus muscle. Reducing RBM20 function in the IG KO mouse by breeding mice with a mouse model that is heterozygous for a deletion in RBM20 (IG KO, RBM20$^{\Delta RRM}$ HET) normalized titin isoform expression. Thus, the reduced size of titin's tandem Ig segment in IG KO mice triggers elevated RBM20 protein levels, which further reduces the size of titin and increases passive stress. The implications of these findings for understanding and treating skeletal myopathies with altered passive stress are discussed.

MATERIALS AND METHODS

Animals

IG KO mice were created by deletion of titin exons 30–38, which correspond to nine proximal Ig domains (Ig 3–11). For details see Chung et al. (2013). Only male mice were used for experiments and studied at 3 mo of age unless otherwise indicated. *Ankrd1* mice were generated in the University of Arizona (UA) BIO5 GEMMCore from embryonic stem cells obtained from the KOMP consortium (http://www.knockoutmouse.org/); the *MARP1* gene (encoding the *Ankrd1* protein) was targeted using the VelociGene technique with the ZEN-UB1 cassette. RBM20$^{\Delta RRM}$ mice were made at the UA BIO5 GEMMCore using homologous recombination. Exons 6 and 7 from the RBM20 mouse gene were deleted causing an in-frame deletion of the RNA recognition motif (RRM). All mouse strains were backcrossed onto a C57BL/6J
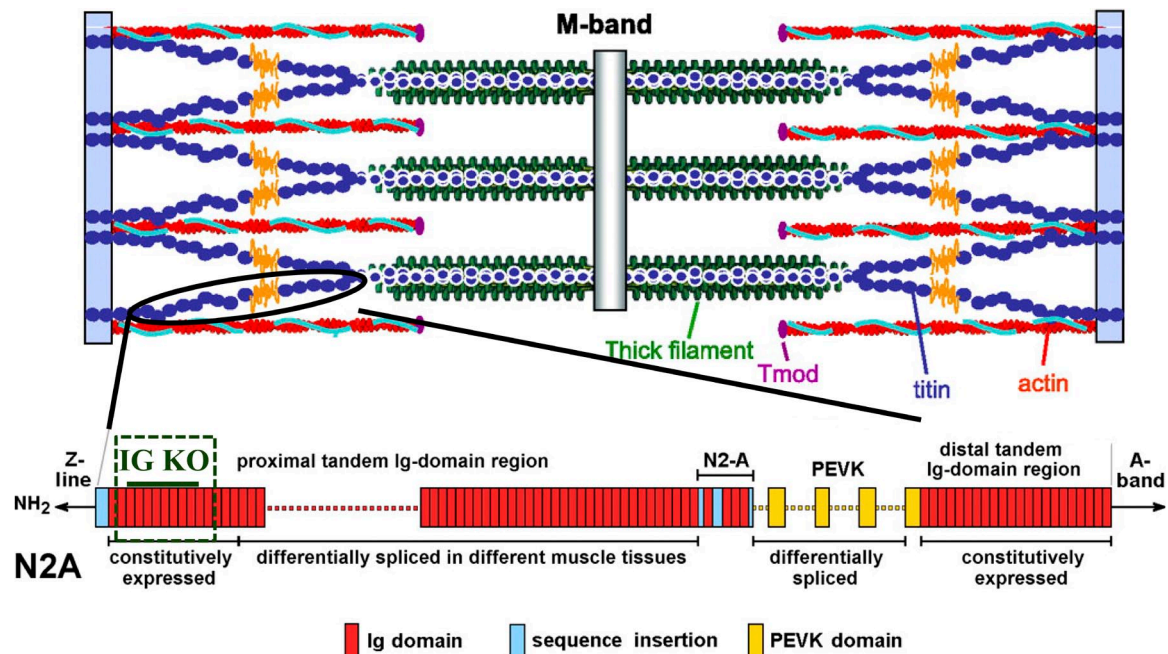
Figure 1. Layout of titin in the sarcomere. A single titin molecule spans the half sarcomere, and its extensible I-band region is composed of Ig-like domains and PEVK sequences that are differentially spliced in skeletal muscles to yield titin isoforms of various sizes. The region of titin that is deleted to produce the IG KO is formed by the constitutively expressed exons 30–38 (Ig 3–11), which is expected to reduce titin size by 88 kD.

genetic background. All animal experiments were approved by the UA Institutional Animal Care and Use Committee and followed the US National Institutes of Health "Using Animals in Intramural Research" guidelines for animal use.

Genotyping

All mice were genotyped using GoTaq Green Master Mix (Promega). For IG KO mice the following primers were used: Common, 5′-GCAGCTACCCATATCATAGC-3′; KO specific, 5′-CACTAGCAGGAACATGTGTC-3′; and WT specific, 5′-GAACGGTGTGGAGATCAAGT-3′; expected product sizes: 319 (WT) and 268 bp (KO). For *Ankrd1* mice the following primers were used: Common, 5′-TCACTAGAGGATATTTTAACACC-3′; KO specific, 5′-TCATTCTCAGTATTGTTTTGCC-3′; and WT specific, 5′-CAGTCACCCGGAAGTCAAA-3′; expected product sizes: 318 (WT) and 286 bp (KO). For RBM20$^{\Delta RRM}$ the following primers were used: Common, 5′-ATATCTGCACCCATGTTTAGTTTCC-3′; KO specific, 5′-GAAGCCAGTGTGTTGGTATGG-3′; and WT specific, 5′-GTGGCCAGCCACGATAGC-3′; expected sizes: 498 (WT) and 817 bp (KO).

Kyphosis index

To quantify spinal shape, animals were anesthetized with Avertin via i.p. injection. Animals were imaged on a GE Healthcare Lunar PIXImus and scanned. Animals were placed on their side in a right lateral recumbent position, and their ventral side was aligned using a straight template. Analysis of the high-energy image of a DXA scan was captured using PIXImus software analyzed offline by manual tracing of images. The lower-energy image showing body composition was not used for this study. Kyphosis index was used as described by others (Laws and Hoey, 2004) and measured as AB/CD, where AB is the distance between the posterior edge of C7 and posterior edge of L6 and CD is the distance from line AB to the distal border of the vertebral body farthest from the line (Fig. S1).

Fiber cross-sectional area (CSA) analysis

The soleus muscle was dissected and pinned onto cork at slack length. The tissue was then covered with OCT (Tissue-Tek) and frozen with liquid nitrogen–cooled isopentane and stored at −80°C. The belly of the muscle was cut crosswise, and 8-µm sections were collected on VWR glass microscope slides and stored at −20°C overnight. The microscope slides were then taken out and left to dry for 5 min. An ImmEdgePen (Vector Laboratories) was used to mark a circle around each section collected. Sections were skinned with 0.2% Triton in PBS for 20 min, followed by treatment with blocking solution (2% BSA and 1% donkey serum) in PBS at 4°C for 1 h. Primary antibodies were then applied to the sections (Table S1) overnight at 4°C. The monoclonal anti-Myosin (skeletal, slow, myosin heavy chain I [MHC-I]; M8421; Sigma-Aldrich) recognizes an epitope located on the heavy meromyosin portion of human adult skeletal muscle slow myosin. The MHC-II antibody (M1570; Sigma Aldrich) stains the fast (type II) and neonatal isomyosin molecules found in skeletal muscle. After primary incubation, sections were washed with PBS twice for 30 min, secondary antibody was applied (2–4 h at room temperature), and they were washed with PBS for 30 min and then washed twice with water. Mounting media (K0424; Vector Laboratories) was then added to each section and sealed with a coverglass. Images were collected on an Axio Imager M.1 microscope (Carl Zeiss) using an Axio Cam MRC (Carl Zeiss). CSAs of the slow and fast myosin fibers were measured using the ImageJ program (National Institutes of Health). Stained cells were traced manually, and the CSAs were determined. The CSAs of ∼150 fibers of each fiber type from the soleus muscle were collected from two to four stained sections, and the total number of fibers in soleus muscle was counted.

Gel electrophoresis and Western blotting

Titin was visualized on 1% agarose gels (16 × 18 cm) stained with Coomassie blue as described previously (Warren et al., 2003). Total titin/MHC ratios and molecular weight estimates have been described previously (Buck et al., 2010). MHC isoform composition was visualized using 8% acrylamide gels (16 × 18 cm; Agbulut et al., 2003). For Western blotting of titin, 0.8% agarose gels (16 × 18 cm) were ran for 3 h at 15 mA/gel and transferred to polyvinylidene fluoride membrane using a semi-dry transfer unit (Bio-Rad Laboratories) for 2.5 h at 150 mA. Western blots of titin-binding proteins were performed with 12% acrylamide gels, except RBM20, calpains, and obscurin, in which 4–20% acrylamide gels were used (13.3 × 8.7 cm; Criterion Cassettes; Bio-Rad Laboratories). All transferred blots were stained with Ponceau S to visualize total transferred protein. The blots were then probed with primary antibodies (Table S1) at 4°C overnight. To normalize for loading differences, actin from the Ponceau S–stained membrane was used unless otherwise indicated. Secondary antibodies conjugated with fluorescent dyes with infrared excitation spectra were used for detection. One-color IR Western blots were scanned (Odyssey Infrared Imaging System; LI-COR Biosciences), and the images were analyzed with One-D scan EX (Scanalytics Inc.).

Microarray

Soleus muscles were collected from WT and IG KO mice ($n = 3$) and stored in RNAlater (Ambion). RNA was isolated using the RNeasy Fibrous Tissue Mini kit (QIAGEN). A custom microarray with all titin exons has been described previously (Lahmers et al., 2004; Ottenheijm et al., 2009b). RNA was reverse transcribed and amplified using SenseAmp (Genisphere) and SuperScript III (Invitrogen) and dye-coupled with Alexa Fluor 555 or Alexa Fluor 647 (Invitrogen). Sample pairs were hybridized with 70 SlideHyb Glass Array Hybridization Buffer #1 (Ambion) in a GeneTAC Hybridization Station (Genomic Solutions); slides were scanned with an Axon GenePix scanner, and the results were analyzed using the R package CARMA (Greer et al., 2006). For Affymetrix microarray analysis, soleus muscle tissue was dissected ($n = 3$) and stored in Ambion RNAlater (Invitrogen). RNA quality was assessed by NanoDrop 1000 Spectrophotometer and 2100 Bioanalyzer (Agilent Technologies); all samples had RIN 9.0–9.3. Samples were hybridized with the GeneChip Mouse Gene 1.0 ST Array (Affymetrix); processing (labeling through scanning) was performed by the Genomics Core, UA, according to Affymetrix protocols and using Affymetrix supplies and equipment. Data analysis was conducted using three different packages: Expression Console (Affymetrix) with RMA, BRB-ArrayTools (Biometric Research Branch, National Cancer Institute) with RMA, and Gene Array Analyzer (http://gaa.mpi-bn.mpg.de/) with either PLIER or RMA. The criteria for a significant difference was that the gene was significantly changed in analysis with all three packages ($P < 0.001$) and had a fold change greater than two between IG KO and WT samples.

Passive and active stress characteristics

Intact muscle mechanics analysis was performed using the Aurora 1200A in vitro test system and has been described previously (Ottenheijm et al., 2009a; Labeit et al., 2010). In brief, soleus muscle was attached between a combination servomotor-force transducer and fixed hook via silk suture in a bath containing oxygenated Ringer solution (145 mM NaCl, 2.5 mM KCl, 1.0 mM MgSO$_4$, 1.0 mM CaCl$_2$ × 2H$_2$O, 1.0 mM HEPES, and 10 mM glucose, pH 7.4, 30°C). For passive force, the muscle was stretched from slack length to 10, 20, and 30% of the muscle length at 10%/s. The muscle was held for 60 s and then returned to slack length, waiting 7 min between each stretch. Measured force in millinewtons was normalized to CSA (muscle mass [mg]/(L0 [mm] × 1.056) to obtain stress (mN/mm^2). The optimal length (L0) was determined by adjusting muscle preload force until optimal fiber length for maximal twitch force was achieved (pulse duration of 200 µs with biphasic polarity).

Active stress was determined from a force-frequency protocol. The muscle was then stimulated at incremental stimulation frequencies 1, 10, 20, 30, 50, 70, 100, and 150 Hz, waiting 30, 30, 60, 90, 120, 120, and 120 s, respectively, in between each activation. From these data, maximal tetanic force, tetanic half-relaxation time, and twitch potentiation were calculated.

The procedures for skinned muscle contractility were as described previously (Granzier and Irving, 1995; Fukuda and Granzier, 2005), with minor modifications. Soleus muscles were skinned overnight at ~4°C in relaxing solution (mM: 20 BES, 10 EGTA, 6.56 MgCl$_2$, 5.88 NaATP, 1 DTT, 46.35 K-propionate, and 15 creatine phosphate, pH 7.0 at 20°C) containing 1% (wt/vol) Triton X-100. Preparations were washed thoroughly with relaxing solution and stored in 50% glycerol/relaxing solution at −20°C. All solutions contained protease inhibitors (in mmol/liter: 0.01 E64, 0.04 Leupeptin, and 0.5 PMSF). Small muscle bundles (diameter ~0.06 mm) were dissected from the skinned muscles. Muscle bundles were attached to a strain gauge and a high-speed motor using aluminum foil clips. Experiments were performed at 20°C. SL was measured online by laser-diffraction using a He-Ne laser beam. The width and depth (using a prism) bundle diameters were measured with a 40× objective. The muscle bundle CSA was calculated from the mean of three width and depth measurements made along the length of the muscle bundle, and passive stress was determined by dividing the passive force by CSA. Muscle bundle length was activated in pCa4.5 activating solution (mM: 40 BES, 10 Ca-EGTA, 6.29 MgCl$_2$, 6.12 Na-ATP, 1 DTT, 45.3 potassium-propionate, and 15 creatine phosphate) and protease inhibitors (mM: 0.01 E64, 0.04 Leupeptin, and 0.5 PMSF) at SL 2.4 µm to record maximal active stress. The bundles were then set at slack in relaxing solution, and passive force was recorded while SL was increased to 3.0 µm (velocity, 0.1 muscle length/s), after which length was held constant for 60 s to observe stress relaxation, followed by a release to slack SL. Subsequently, thick and thin filaments were extracted by immersing the preparation in relaxing solution containing 0.6 M KCl (45 min at 20°C), followed by relaxing solution containing 1.0 M KI (45 min at 20°C). After the extraction procedure, the muscle bundles were stretched again at the same velocity, and the passive force remaining after KCl/KI treatment was assumed to be collagen based, and titin-based passive force was determined as total passive force minus collagen-based passive force.

Statistics

All data are represented as mean ± SEM. For data with numbers of mice (n) greater than or equal to eight, an unpaired t test with a p-value <0.05 was considered significant. For experiments performed with data less than eight, a Mann–Whitney test, which does not assume Gaussian distributions, was performed (P < 0.05 significant). For MHC isoform analysis, active specific tension, and passive stress analysis, two-way ANOVA with a Bonferroni post-test was performed (P < 0.05 significant). For all figures: *, P < 0.05; **, P < 0.01; ***, P < 0.001.

Online supplemental material

Figures showing the kyphosis analysis (Fig. S1), titin size analysis during development (Fig. S2), examples of Western blot results for titin-binding antibodies (Fig. S3), and single fiber protein analysis (Fig. S4) are included. A list of the antibodies used can be found in Table S1. Online supplemental material is available at http://www.jgp.org/cgi/content/full/jgp.201311129/DC1.

RESULTS

Phenotypic characterization of IG KO mice

Mice deficient in Ig domains 3–11 of titin's proximal tandem Ig segment (IG KO) have recently been shown to have a mild cardiac diastolic phenotype (Chung et al., 2013), but the role of these proximal Ig domains in skeletal muscle had not been studied. Upon more detailed characterization, it was found that IG KO mice displayed

TABLE 1

Muscle weight measurements of WT and IG KO mice

Parameter	WT	KO	P-value	% Change
Age (d)	94.38 ± 1.2 (41)	93.29 ± 1.2 (43)		
Body weight (g)	25.2 ± 0.4 (41)	21.6 ± 0.5 (41)	<0.001	−13.98
Tibia length (mm)	17.8 ± 0.03 (21)	17.6 ± 0.06 (21)		−1.02
Wet weight				
Soleus (mg)	8.7 ± 0.2 (30)	7.3 ± 0.1 (23)	<0.01	−15.65
TC (mg)	48.3 ± 0.5 (30)	49.3 ± 0.9 (23)		2.07
Quadriceps (mg)	194 ± 2.7 (30)	184 ± 3.4 (23)		−5.39
EDL (mg)	10.9 ± 0.1 (30)	10.6 ± 0.1 (23)		−2.23
Gastrocnemius (mg)	127 ± 1.2 (30)	126 ± 1.7 (23)		−1.24
Plantaris (mg)	16.9 ± 0.2 (30)	16.5 ± 0.2 (21)		−2.59
Diaphragm (mg)	80.8 ± 2.1 (38)	69.1 ± 1.7 (40)	<0.001	−14.42
Psoas (mg)	82.4 ± 2.2 (16)	77.9 ± 2.6 (14)		−5.42
Tibia length normalized				
Soleus (mg/mm)	0.51 ± 0.013 (21)	0.41 ± 0.009 (21)	<0.001	−18.61
TC (mg/mm)	2.75 ± 0.03 (21)	2.79 ± 0.04 (21)		1.57
Quadriceps (mg/mm)	10.9 ± 0.15 (21)	10.4 ± 0.16 (21)		−4.41
EDL (mg/mm)	0.62 ± 0.005 (21)	0.60 ± 0.009 (21)		−3.23
Gastrocnemius (mg/mm)	7.29 ± 0.06 (21)	7.16 ± 0.08 (21)		−1.81
Plantaris (mg/mm)	0.97 ± 0.01 (21)	0.93 ± 0.01 (19)		−4.36
Diaphragm (mg/mm)	4.47 ± 0.10 (19)	3.97 ± 0.12 (17)	<0.01	−11.20
Psoas (mg/mm)	4.91 ± 0.11 (9)	4.53 ± 0.14(14)		−7.81

n values are shown in parentheses. Percent change is calculated as [(KO − WT)/WT] × 100.
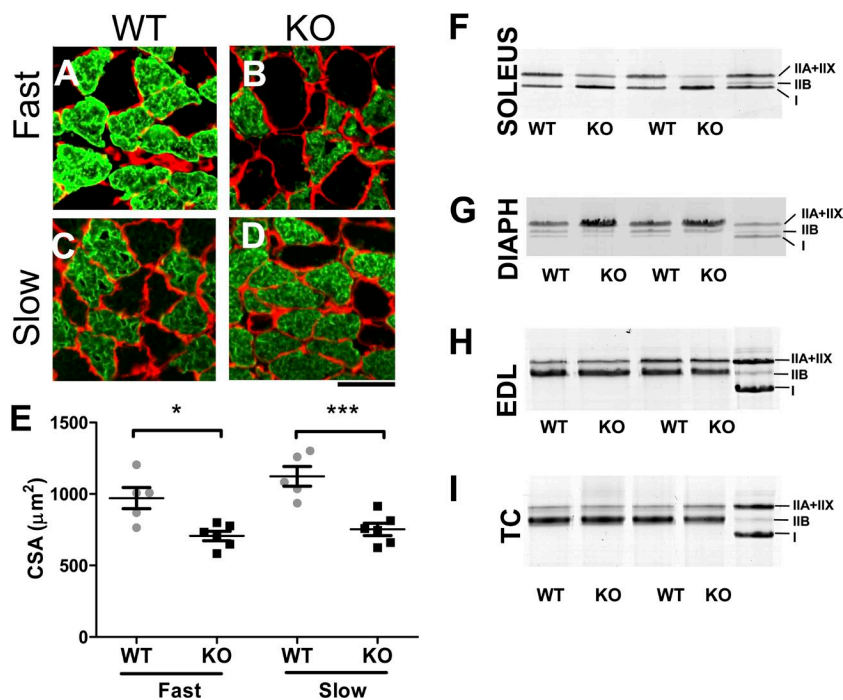
Figure 2. Soleus muscle fibers from IG KO mice have a decrease in fiber CSA and an increase in slow MHC isoform composition. (A–D) Fast and slow myosin fibers were stained separately (green), with cell boundaries marked by laminin (red). Bar, 50 µm. (E) CSA of muscle fibers was quantified from $n = 5$ WT and 6 IG KO mice ($n = 250$ fibers per mouse). Data show mean ± SEM. *, $P < 0.05$; ***, $P < 0.001$. (F–I) MHC isoform composition from soleus, diaphragm, TC, and EDL.

a slight but significant spine curvature (kyphosis) as quantified by the kyphosis index (Fig. S1). Kyphosis is a commonly associated phenotype in mouse models of disease in which skeletal muscles are affected (Laws and Hoey, 2004; Witt et al., 2004). Compared with the kyphosis of other muscle disease models, the kyphosis in the IG KO was less prominent but nevertheless suggested that the IG KO mouse model outwardly displayed signs that could be associated with skeletal muscle myopathy. This prompted us to look at the effect of this deletion in skeletal muscle.

Analysis of skeletal muscle mass revealed that the soleus and diaphragm muscles from IG KO mice were significantly smaller (raw weight and normalized to tibia length; Table 1), whereas all other muscles exhibited no difference. In the mouse, most muscle types express mainly fast MHC. The two well-known exceptions that express a greater abundance of slow MHC are the soleus and diaphragm muscle (Agbulut et al., 2003), and this suggested that there may be fiber type specificity to the atrophy phenotype whereby slow myosin-expressing fibers (type I) were more affected than fast myosin-expressing fibers (type II). We therefore measured the fiber CSA of type I and type II fibers from soleus muscle using immunofluorescence (Fig. 2). Interestingly, both fast and slow muscles underwent similar fiber atrophy (37.9% and 49.7%, respectively), indicating that the atrophy observed in the soleus muscle was not caused by effects specific to slow myosin-expressing muscle. Additionally, we found that the total number of muscle fibers was not different (not depicted), supporting the idea that atrophy of the muscle was caused by a decrease in the size of fibers. Gel electrophoresis of MHC isoforms revealed an

increase in slow MHC in the IG KO soleus muscle (Fig. 2 F and Table 2). This shift in MHC isoform composition is likely part of a compensatory mechanism that develops postnatally as no shift in MHC isoform composition was observed in neonatal day five soleus muscle (Table 2). This isoform shift to a slow myosin isoform composition appeared to be soleus muscle specific as a survey of various skeletal muscles showed either no significant difference (tibialis cranialis [TC] and extensor digitorum

TABLE 2

MHC isoform composition as quantified by Coomassie stain of protein lysates

Muscle	IIA + IIX	IIB/N	I
	%	%	%
Soleus (3 mo)			
WT	60 ± 2.2	2 ± 0.5	37 ± 2.3
KO	40 ± 3.1[a]	2 ± 0.4	57 ± 2.8[a]
Diaphragm (3 mo)			
WT	76 ± 2.8	16 ± 3.4	6.8 ± 0.9
KO	85 ± 4.9	12 ± 5.1	1.5 ± 0.5[b]
EDL (3 mo)			
WT	17 ± 1.2	82 ± 1.2	0
KO	19 ± 1.2	80 ± 1.2	0
TC (3 mo)			
WT	23 ± 5.1	76 ± 5.1	0
KO	28 ± 6.7	71 ± 6.7	0
Soleus (5 d)			
WT	35 ± 1.6	45 ± 1.4	18 ± 0.1
KO	34 ± 1.7	49 ± 1.4	15 ± 0.2

Data are represented as percentage of total MHC ($n = 8$ WT and 8 KO).
[a]$P < 0.001$.
[b]$P < 0.01$.
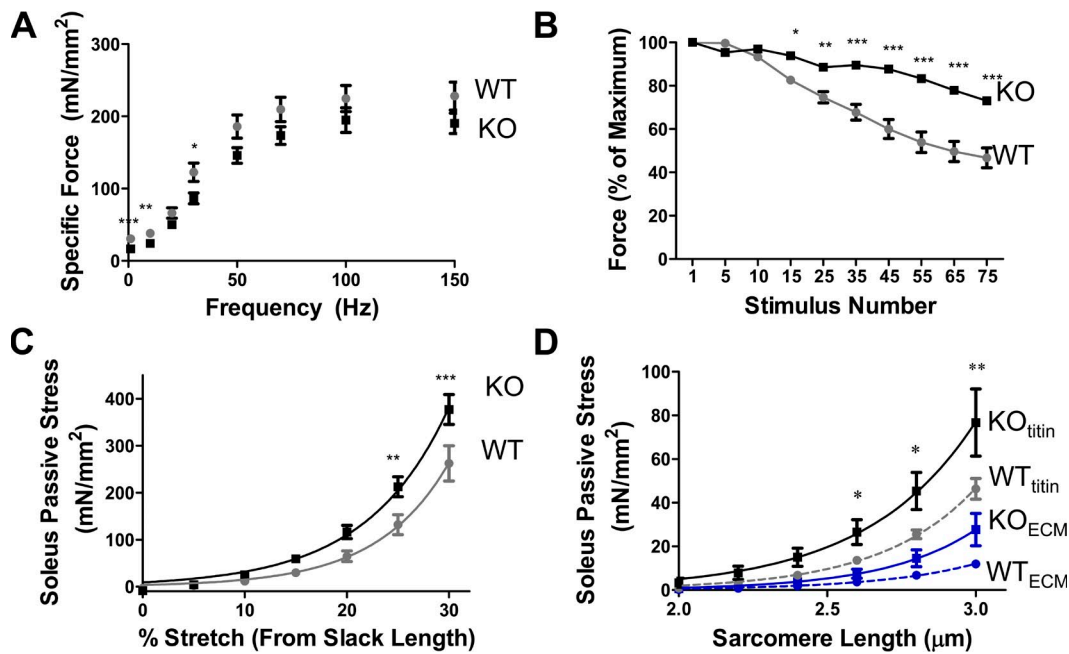
Figure 3. Active and passive mechanics from IG KO and WT soleus muscle. (A) Force-frequency relation of IG KO and WT mice. (B) IG KO muscle is more resistant to fatigue. (C) Intact soleus muscle passive stress is significantly increased in IG KO mice. (D) Skinned fiber bundles were dissected from the soleus muscle and passively stretched, followed by extraction with KCl/KI, and were restretched. Titin-based passive stress is defined as total stress minus the extracted stress. The increase in passive stress in the soleus is attributed to an increase in titin-based passive stress. Data show mean ± SEM. *, P < 0.05; **, P < 0.01; ***, P < 0.001.

longus [EDL]) or a significant decrease in slow MHC (diaphragm; Fig. 2, G–I; and Table 2).

Muscle mechanics reveal changes in skeletal muscle contractility

The changes in MHC isoform composition in soleus muscle of IG KO mice suggest that there may be changes in contractility of the soleus muscle. Slow myosin fibers differ from fast fibers in that they are more oxidative, have a lower power output, and resist fatigue (Rivero et al., 1998). Results from intact mechanics of soleus muscle showed that IG KO mice had a significant decrease in twitch force (Fig. 3 A and Table 3) and were more resistant to fatigue (Fig. 3 B). These findings are

TABLE 3
Active force measurements in soleus muscle of IG KO and WT mice

Parameter	WT	KO	P-value
Maximal force (g)			
Twitch	2.48 ± 0.21	1.20 ± 0.084	<0.001
Tetanus	16.70 ± 1.36	11.59 ± 0.68	<0.01
CSA (mm²)	0.72 ± 0.03	0.63 ± 0.01	<0.01
Maximal stress (mN/mm²)			
Twitch	33.6 ± 2.5	18.9 ± 1.3	<0.001
Tetanus	226 ± 17	184 ± 13	0.06
Twitch/tetanus ratio	0.134 ± 0.006	0.086 ± 0.004	<0.001
Time to Peak (s)			
Twitch	0.025 ± 0.001	0.026 ± 0.001	0.62
Tetanus	0.844 ± 0.06	0.643 ± 0.06	<0.05
1/2 Relaxation time (s)			
Twitch	0.0275 ± 0.001	0.035 ± 0.002	<0.001
Tetanus	0.049 ± 0.002	0.055 ± 0.003	0.11
Post-tetanic twitch potentiation	0.96 ± 0.01	0.98 ± 0.01	0.26
Frequency at 1/2 max force (Hz)	76.1 ± 2.28	70.7 ± 5.86	0.43
Force decrease during fatigue (%)	0.53 ± 0.05	0.27 ± 0.02	<0.001

n = 9 WT and 9 KO.
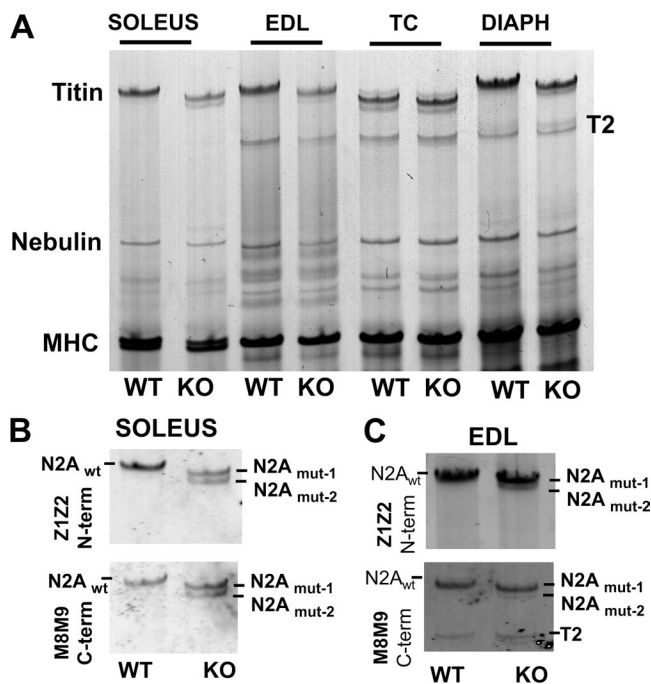
Figure 4. Additional differential splicing occurs in IG KO skeletal muscle. (A) Agarose gel electrophoresis shows additional titin bands present in skeletal muscle from IG KO mice. (B and C) These additional bands are positive for titin's N terminus (Z1Z2) and C terminus (M8M9) and therefore represent full-length titin isoforms.

likely to reflect the change in MHC isoform composition from fast to slow. Passive properties of intact muscle were also studied. The soleus muscle contains one of the largest titin isoforms of adult striated muscle (Labeit and Kolmerer, 1995), and the deletion of nine proximal Ig domains is expected to have a minimal effect on passive stress (the effect is a ∼2% stress reduction in the much smaller cardiac N2B titin [Chung et al., 2013]). However, passive stress in the intact soleus muscle was significantly increased in the KO, when stretched from its slack length, to a level much greater than in WT muscle (mean of 30.9 ± 0.2% change; Fig. 3 C). A similar increase in passive stress also occurred in the EDL muscle (not depicted). Thus, passive stress of skeletal muscle is increased in IG KO mice but to an extent greater than expected by the deletion of only nine proximal Ig domains.

At the level of the intact muscle, the extracellular matrix (ECM) contributes to passive stress in addition to titin and could have been the cause of the greater than expected increase in passive stress. To distinguish between these two contributors, skinned fibers were studied. Demembranized fiber bundles were passively stretched to determine the total stress, followed by an extraction of thin and thick filament proteins with KCl/KI to remove titin's anchoring points in the sarcomere (Wu et al., 2002). The fiber bundle was passively stretched again to determine the nontitin, ECM passive stress contribution. Titin-based stress is defined as the difference between

total stress and ECM-based stress. No difference in maximal activated stress was observed between genotypes, consistent with the tetanic stress observed in intact soleus muscle (153 ± 7.5 mN/mm^2 WT vs. 151 ± 13 mN/mm^2 KO). The soleus muscle from IG KO mice was found to have a significant increase in titin-based passive stress above 2.5 µm SL, whereas the ECM was not significantly increased (Fig. 3 D). The mean percent change (defined as ((KO-WT)/WT) × 100) in titin-based passive stress is 30.2 ± 2%, similar to that observed in intact muscle. These results indicate that the large increase in passive stress observed in intact muscle reflects an increase in titin-based passive stress.

IG KO mice undergo additional alternative splicing of titin in skeletal muscles

Titin-based passive stress can vary through alterations in titin size, phosphorylation status, and titin/MHC stoichiometry (Watanabe et al., 2002; Hidalgo and Granzier, 2013). Because a large increase in passive stress was observed in IG KO mice, we sought to determine the contribution of these various factors to the mechanical properties of muscle. Large pore agarose gels were used to visualize titin isoform size. The genomic region deleted to produce the IG KO was expected to yield a single mutant titin protein 88 kD smaller than WT titin. IG KO mice instead contained two faster-migrating bands (N2A$_{mut-1}$ and N2A$_{mut-2}$) in the soleus, EDL, and diaphragm muscles (Fig. 4 A). The second faster-migrating band was most prominent in the soleus muscle. To test whether this faster-migrating band (N2A$_{mut-2}$) was either a titin degradation product or a full-length titin isoform, Western blots were performed with antibodies raised against titin's N terminus (Z1Z2 antibody) and C terminus (M8M9 antibody). The smaller band contained both of titin's ends in both soleus (Fig. 4 B) and EDL muscle (Fig. 4 C), and thus it is a full-length titin isoform. The molecular weight of the titin isoforms N2A$_{mut-1}$ and N2A$_{mut-2}$ in the soleus muscle was estimated as described previously (Buck et al., 2010). The N2A$_{mut-1}$ and N2A$_{mut-2}$ isoforms were reduced in size by more than the expected 88-kD deletion (Table 4), indicating that

TABLE 4

Mean adult molecular mass estimates of titin

Muscle	WT	KO	ΔMD
	MD	*MD*	
Soleus (N2A$_{wt}$)	3.61 ± 0.057	Not present	
Soleus (N2A$_{mut-1}$)	Not present	3.43 ± 0.008[a]	0.18
Soleus (N2A$_{mut-2}$)	Not present	3.24 ± 0.027[a]	0.37
EDL (N2A$_{wt}$)	3.66 ± 0.087	Not present	
EDL (N2A$_{mut-1}$)	Not present	3.47 ± 0.014[a]	0.19
EDL (N2A$_{mut-2}$)	Not present	3.21 ± 0.003[a]	0.42

n = 4 WT and 4 KO.
[a]P < 0.05.

adaptations in splicing had taken place in the IG KO. Interestingly, these mutant titin isoforms were developmentally regulated; they were not present at birth, and the $N2A_{mut-2}$ over $N2A_{mut-1}$ ratio increased with age (Fig. S2). Thus, changes in splicing that occur postnatally in the IG KO are both progressive and adaptive.

To more directly observe changes in titin splicing, a titin exon microarray analysis was performed on 3-mo-old soleus muscle. As expected, the nine Ig domains removed in the IG KO (exons 30–38) were absent (Fig. 5 A). In the IG KO soleus muscle, there was also a down-regulation in exons that encode PEVK sequences. This down-regulation was confirmed at the protein level via Western blots performed using the 9D10 antibody (Fig. 5, B and C). This antibody recognizes repetitive sequences throughout the entire PEVK region (Trombitás et al., 1998; Greaser et al., 2000). There was a decrease in labeling of the two mutant titin isoforms with the 9D10 antibody in the IG KO as normalized to total titin (Z1Z2 antibody), supporting the idea that the difference in isoform size was, at least in part, caused by additional differential splicing in the PEVK region of titin.

In addition to alternative splicing, titin-based passive stress can also be modulated by phosphorylation. Skeletal muscle titin is a target of phosphorylation by PKC-α in the PEVK domain. Phosphorylation of two serines (PS11878 and PS12022) has previously been shown to significantly increase passive stress (Hidalgo et al., 2009). Phosphorylation of titin at serine 11878 was significantly reduced in IG KO soleus muscle, whereas phosphorylation at serine 12022 was unchanged (Fig. 6); the expected net effect of this reduction in phosphorylation is a lower passive stress. This expected effect will partially offset the passive stress increase produced by the reduction in titin size caused by differential splicing in the IG KO (see also Discussion).

The amount of titin relative to the sarcomeric protein myosin reflects the stoichiometry of titin to thick filaments. Total titin/MHC ratios were not significantly different between genotypes in all muscles observed (Table 5). This indicates that the deletion of Ig domains in the IG KO did not affect the number of titin filaments per thick filament. The titin degradation product, T2, was also not significantly altered by Ig domain deletion (Table 5). In summary, soleus muscle titin from IG KO mice undergo additional alternative splicing and alterations in phosphorylation.

Titin-binding proteins in IG KO soleus muscle

It has been proposed previously that titin-binding proteins can function in signalosomes to sense strain and modulate protein expression (LeWinter and Granzier, 2010; Linke and Krüger, 2010), and it has been hypothesized that changes in these signalosomes could be responsible for changes in gene expression. Titin-binding protein abundance was assayed by Western blot analysis in the soleus muscle, and it was found that proteins that bind in the I-band region were differentially regulated, whereas those in the M line and A band were less affected (Fig. 7 and Fig. S3). The calpain (CAPN) family are a group of calcium-dependent intracellular proteases, some of which bind titin in the N2A region (calpain-3; Hayashi et al., 2008) or the proximal Ig domains (calpain-1, binding site deleted in IG KO; Coulis et al., 2008; Sorimachi et al., 2011). CAPN1 (catalytic subunit of calpain-1) amount was quantified by antibodies
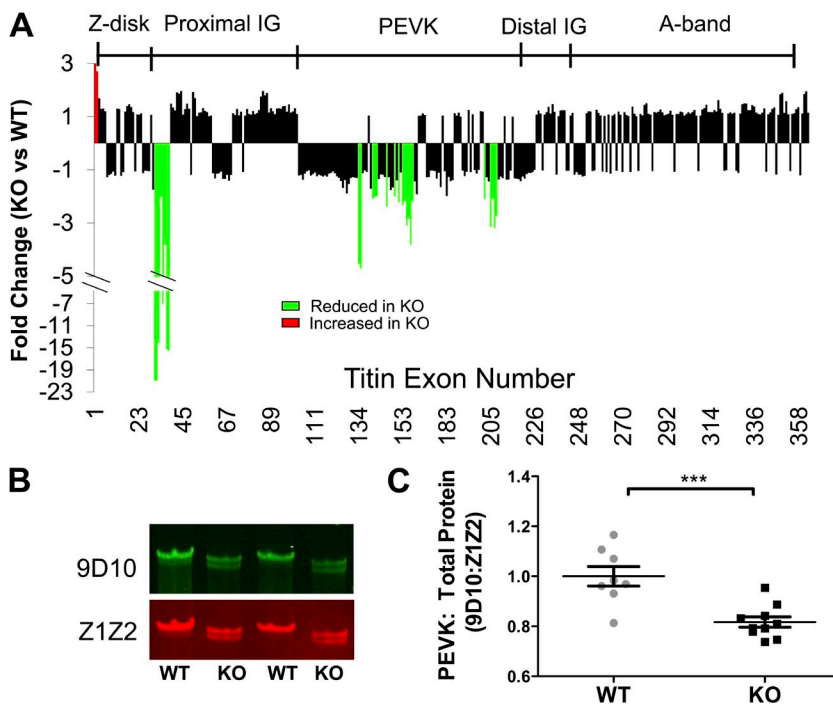
Figure 5. PEVK exons are additionally removed in the IG KO mouse. (A) Custom-made titin exon microarray confirms that the constitutively expressed exons 30–38 are deleted in the soleus muscle of IG KO mice. Additional differential expression was also found to occur in the PEVK region of the titin transcript. (B and C) The removal of PEVK exons was confirmed at the protein level by a significant reduction in 9D10 antibody labeling, which recognizes the highly repetitive sequences within the PEVK region of titin. (For KO samples, we summed the signal from the two mutant titin isoforms.) Data show mean ± SEM. ***, P < 0.001.
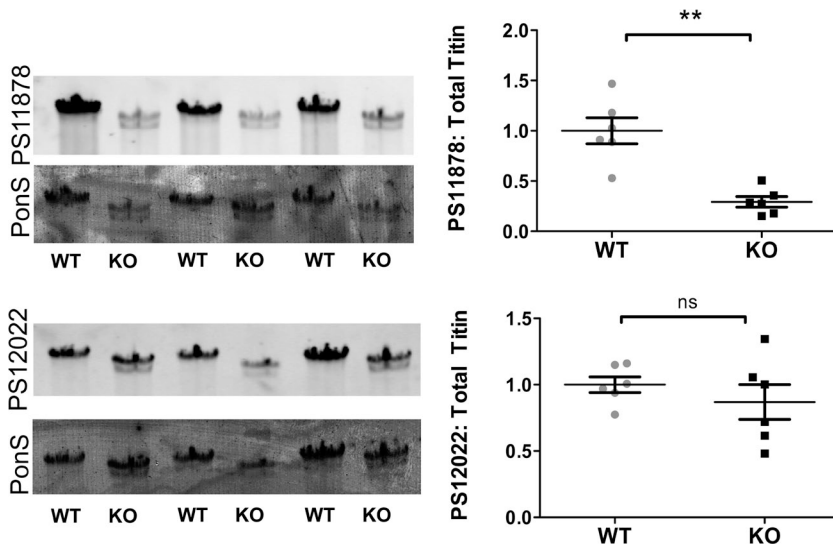
Figure 6. PKC-α targets two serines in the PEVK region of titin (S11878 and S12022). Titin phosphorylation at PS11878, but not PS12022, is significantly reduced in IG KO mice. Data show mean ± SEM. **, P < 0.01.

against the full-length inactive CAPN1 (pre-calpain) and self-autolysis–activated CAPN1 (post-calpain; Saido et al., 1992). There was no significant difference between active and inactive forms of calpain-1 between WT and IG KO mice in soleus muscle. There was also no significant difference in the amount of calpain-3 present between genotypes (Fig. 7). Of the proteins that bind titin's I band, FHL-1 and FHL-2 were modestly up-regulated, whereas *Ankrd2* (also called MARP2) and *Ankrd3* (DARP/MARP3) were modestly down-regulated in 3-mo-old IG KO soleus muscle as compared with WT (Fig. 7). Most dramatic was the induction of *Ankrd1* (CARP [cardiac ankyrin repeat protein]), which was up-regulated in the IG KO soleus muscle >60-fold (Fig. 7).

Ankrd1 expression is highly increased but does not explain alternative splicing

Ankrd1 was considered a candidate for inducing the additional differential splicing of titin in IG KO mice for several reasons. First, *Ankrd1* is normally expressed at high levels in cardiac muscle where titin size is greatly reduced. Second, mice deficient in the three muscle ankyrin repeat family members, *Ankrd1*, *Ankrd2*, and *Ankrd3* (MKO), displayed an increase in titin size (Barash et al., 2007). Finally, *Ankrd1* can act as a transcription factor in the nucleus to alter gene expression through inhibition of the NF-κB pathway (Laure et al., 2010). If *Ankrd1*

up-regulation were necessary for additional differential splicing to occur, then titin would not undergo additional differential splicing in *Ankrd1*-deficient IG KO mice. To test this, *Ankrd1* KO mice were bred to IG KO mice to produce double KOs. Mice were studied at 1 mo of age, a time when the N2A$_{mut-2}$ isoform is present. As highlighted in Fig. 8, deletion of *Ankrd1* did not prevent the additional differential splicing, and both N2A$_{mut-1}$ and N2A$_{mut-2}$ were expressed in the double KO mice.

RBM20 expression is up-regulated in IG KO mice

Recently, it has been uncovered that the splicing factor RBM20 plays a role in regulating alternative splicing of titin, with an increase in RBM20 expression leading to exclusion of PEVK exons in a splice reporter assay (Guo et al., 2012). A 2.1-fold increase in RBM20 was found in IG KO soleus muscle relative to WT (Fig. 9, A–C). RBM20 expression was normalized to both MHC and another nuclear splicing factor U2AF65, as performed by others (Li et al., 2013), but the same result was found. These findings support the idea that RBM20 up-regulation leads to exclusion of PEVK exons in titin.

To identify potential pathways in which increased titin-based stress leads to up-regulation of RBM20 and additional differential splicing, an Affymetrix GeneChip was used. The microarray analysis found 28 mRNA transcripts

TABLE 5

Stoichiometry of titin

Muscle	Total titin/MHC			T2: Total titin		
	WT	KO	P-value	WT	KO	P-value
Soleus	0.194 ± 0.019	0.188 ± 0.030	NS	0.012 ± 0.006	0.025 ± 0.004	NS
TC	0.293 ± 0.025	0.303 ± 0.039	NS	0.224 ± 0.043	0.281 ± 0.031	NS
EDL	0.183 ± 0.013	0.205 ± 0.008	NS	0.330 ± 0.022	0.296 ± 0.005	NS
Diaphragm	0.192 ± 0.028	0.194 ± 0.031	NS	0.200 ± 0.043	0.304 ± 0.156	NS

n = 8 per genotype and muscle type.

significantly altered in IG KO mice. Many of the genes identified in the Affymetrix microarray reflect the transition to a more slow fiber phenotype. These include up-regulation of mitochondrial gene UCP2 and down-regulation of genes expressed in fast fiber types, including Myoz1, Kcng4, Peg3, Myom2, and Nos1 (Grozdanovic and Baumgarten, 1999; Chemello et al., 2011). Among the 28 differentially expressed transcripts, only two transcription factors were found: *Ankrd1* and Runx1 (Fig. 10). Runx1, a transcription factor which regulates blood cell differentiation (Friedman, 2009), is unlikely to be responsible for changes in skeletal muscle titin. Furthermore, we found no Runx1-binding sites within the RBM20 promoter region (not depicted). These data suggest that the transcription factor that is responsible for up-regulation of RBM20 might not be regulated at the level of mRNA expression.

RBM20 is necessary for the additional differential splicing in IG KO soleus muscle

To test whether RBM20 activity is necessary for additional differential splicing, IG KO mice were crossed with mice deficient in the RRM domain of RBM20 (RBM20$^{\Delta RRM}$). Mice heterozygous for RBM20$^{\Delta RRM}$ displayed a single titin band intermediate of the titin band in mice that were either WT or homozygous for the RBM20$^{\Delta RRM}$ (Fig. 9 D). This is consistent with what has

been shown previously in the rat model with a spontaneous mutation in RBM20 (Guo et al., 2012). These data indicate that RBM20 functions in a dose-dependent manner to regulate differential splicing of titin. In 3-mo-old mice that are deficient in Ig 3–11 and that are heterozygous for RBM20 (IG KO, RBM20$^{\Delta RRM}$ HET), only a single titin bands appears. This data support the interpretation that RBM20 up-regulation is required to cause additional differential splicing of titin in IG KO soleus muscle.

DISCUSSION

We studied skeletal muscle titin in a mouse model deficient in titin's proximal Ig domains Ig 3–11 (IG KO) and found that this deletion unexpectedly results in additional differential splicing in the PEVK region of titin. The splicing was prominently found in the soleus muscle with the appearance of two mutant titin isoforms. These isoforms significantly increased passive stress of whole muscle and caused altered expression of titin-based signaling proteins, with the most striking effect being the 60-fold up-regulation of the transcription factor *Ankrd1*. However, IG KO mice that were also deficient in *Ankrd1* (IG KO, *Ankrd1* KO) showed that *Ankrd1* is not necessary for additional differential splicing. We also found that the additional splicing of titin correlates with an increased level of the RBM20 splicing factor
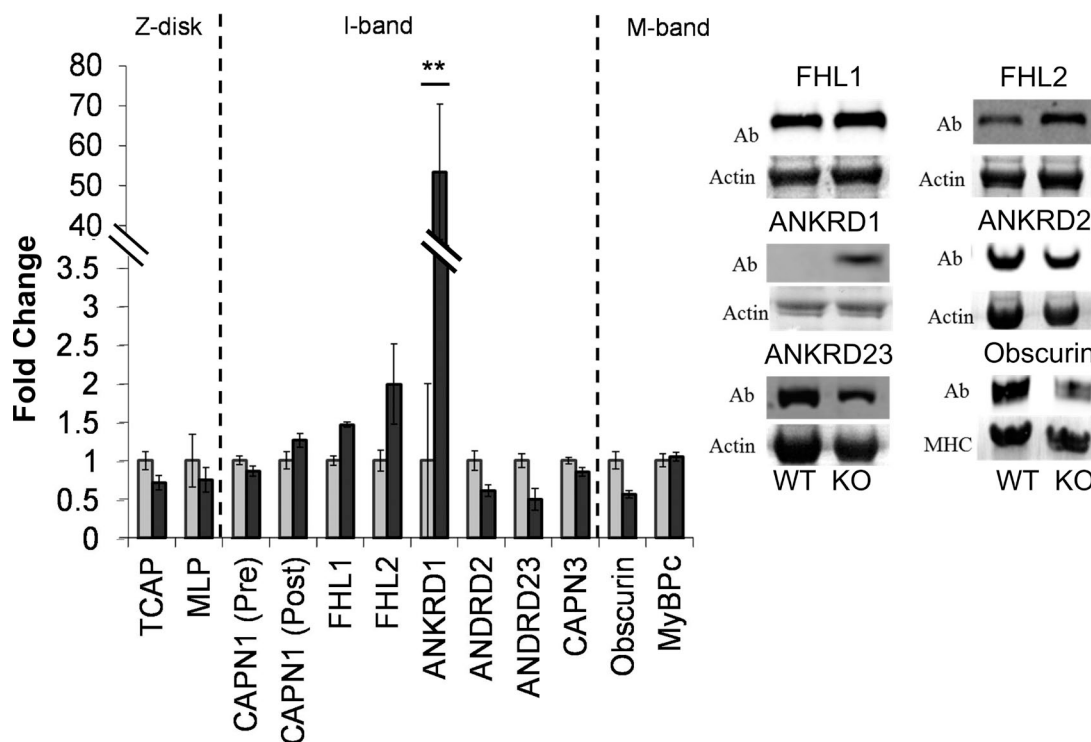
Figure 7. Survey of titin-binding protein expression by Western blot analysis. FHL-1, FHL-2, and *Ankrd1* were significantly up-regulated in IG KO mice, whereas *Ankrd2*, MARP3, and obscurin were significantly down-regulated in IG KO mice. Data are collected from $n = 6$ WT and 6 KO mice. Normalized Western blot signals were calculated by dividing the antibody (Ab) signal by the actin signal, and fold change was normalized to WT levels. Data show mean ± SEM. **, P < 0.01.

and that genetically reducing RBM20 activity in the IG KO mice (IG KO, RBM20$^{\Delta RRM}$ HET) prevents the additional differential splicing from occurring. Thus, RBM20 is a central player in differential splicing of titin mRNA and its expression can be modified by changes in titin-based passive stress to result in shorter and stiffer titins. Below we discuss these findings in detail.

Adaptations in titin splicing in IG KO mice

The most prominent finding from the characterization of skeletal muscles from the IG KO mice was that gel electrophoresis revealed titin isoforms that are smaller in the IG KO, but to a degree that far exceeded the level expected from the deletion of nine Ig domains (88 kD). Specifically, the soleus muscle contains two smaller titin bands with a reduction in size of 180 kD and 370 kD, respectively. A full-length shortened titin isoform would be expected to contain both of titin's ends, but lack centrally located sequences, whereas a degradation product would be expected to miss at least one of titin's ends. Using antibodies against titin's N terminus (Z1Z2) or C terminus (M8M9), it was observed that the two bands in the soleus muscle were both full-length titin isoforms. A titin exon microarray analysis revealed a reduced expression of PEVK exons in titin's I-band region in the IG KO soleus muscle, suggesting that the smaller full-length titin isoforms arose at least in part from the elimination of PEVK exons. However, the reduction in molecular mass estimated from protein gels (N2A$_{mut-2}$ 370 kD) exceeds the maximal molecular mass of the whole PEVK region (~250 kD), suggesting that other effects might be at play. One issue to consider is that the mobility of the PEVK sequence is much slower than that expected based on its molecular mass (Labeit et al., 2003), leading to an overestimation of the molecular mass reduction in the IG KO. Whether some Ig domains
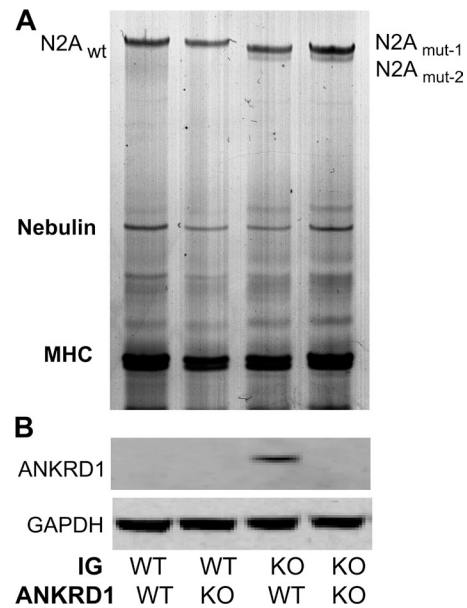
Figure 8. *Ankrd1* is not necessary for additional differential splicing in the IG KO mouse. (A) Mice deficient in both *Ankrd1* and IG domains still have the N2A mutant titin isoforms. (B) Western blot analysis confirms that *Ankrd1* is removed in the double KO mouse.

in the tandem Ig segments are reduced in expression in the IG KO could be addressed in future studies with Ig-domain specific antibodies. In summary, adaptations in splicing take place in the IG KO that decrease titin size in the soleus. This is an unexpected finding that the muscle adapts to a shorter titin by making titin molecules that are even shorter and stiffer.

Soleus muscle from WT mice only displays a single titin isoform, even during development. It is possible that the isoforms of titin observed in the soleus muscle of IG KO mice are restricted to a particular fiber type, whereby
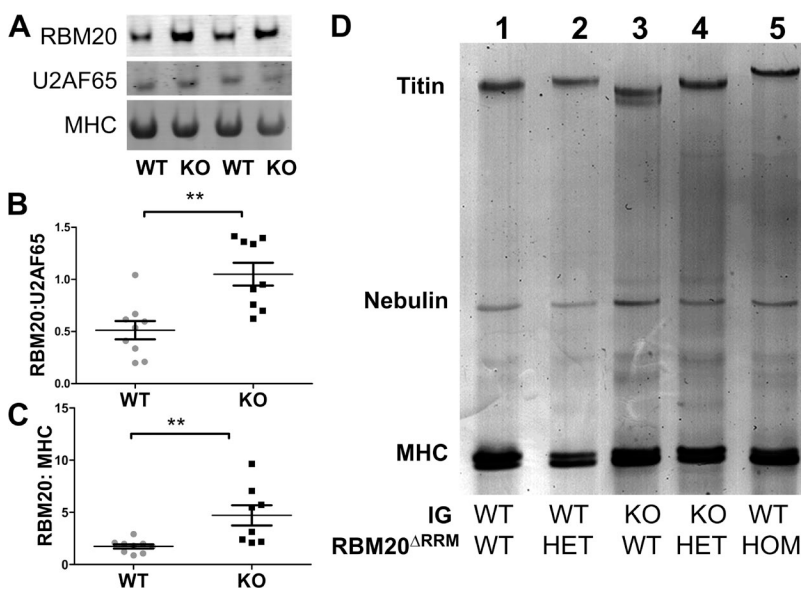
Figure 9. RBM20 is up-regulated in IG KO soleus muscle. (A) Western blots of the titin splicing factor RBM20, with U2AF65 (another splice factor) and MHC (as controls). (B and C) RBM20 expression is significantly up-regulated when normalized to U2AF65 (B) or MHC (C). Data show mean ± SEM. **, P < 0.01. (D) IG KO mice with reduced RBM 20 activity (IG KO × RBM20$^{\Delta RRM}$ HET) have a normalization of titin size (lane 4) similar to that of WT (lane 1).

each fiber only expresses a single titin isoform, giving rise to two titin isoforms at the level of the whole muscle. At 3 mo of age, the N2A$_{mut-2}$ to N2A$_{mut-1}$ ratio was 38%, which resembles very closely the myosin type 1 content of 37% (Table 2). To test this, single fibers from the soleus muscle were dissected and were individually electrophoresed to separate both titin and MHC isoforms. From these experiments, it was found that the titin isoforms were co-expressed in a single fiber, which indicates that titin isoform expression did not segregate with myosin fiber type (Fig. S4). Although we currently cannot exclude a specific location of the mutant isoforms within a single muscle fiber, we consider it likely that similar to the co-expression of cardiac titin isoforms (Trombitás et al., 2001), the mutant skeletal muscle titins are coexpressed at the level of the half sarcomere.

In addition to changes at the mRNA level, posttranslational modification of titin was found to occur in the soleus muscle of IG KO mice, which is expected to influence passive stress. Specifically, phosphorylation at serine 11878 in the PEVK region was reduced, a site which is a target of PKC-α signaling (Hidalgo et al., 2009). Interestingly, phosphorylation at serine 12022, another PKC-α target, was not affected in IG KO mice. The difference in phosphorylation of the two PKC sites is not caused by a difference in expression of the exons because microarray analysis of the titin exons in which these serines are contained (exon 219 and 225, respectively) shows no change in the expression between genotypes; the difference in phosphorylation remains to be explained. Phosphorylation at both of these sites has been shown to increase passive stress of cardiac muscle (Hidalgo et al., 2009; Hudson et al., 2010).

7.0 ■■■■ ▨▨ ■■■ -7.0

Fold-change	Symbol	Description
7.23	Ankrd1	ankyrin repeat domain 1 (cardiac muscle) -- CARP
6.64	Muc15	mucin 15
5.92	Ndrg4	N-myc downstream regulated gene 4
5.50	Ucp2	uncoupling protein 2 (mitochondrial, proton carrier)
3.27	Sln	sarcolipin
3.16	3632451O06	RIKEN cDNA 3632451O06 gene
2.41	Col8a1	collagen, type VIII, alpha 1
2.39	Myl4	myosin, light polypeptide 4
2.36	Ano3	anoctamin 3
2.33	Sesn3	sestrin 3
2.32	Runx1	runt related transcription factor 1
2.22	Pam	peptidylglycine alpha-amidating monooxygenase
2.13	Lrp2bp	Lrp2 binding protein
2.11	Pkp2	plakophilin 2
2.08	Nrcam	neuron-glia-CAM-related cell adhesion molecule
2.00	Peg3	paternally expressed 3
-2.13	Fbp2	fructose bisphosphatase 2
-2.13	Myom2	myomesin 2
-2.22	Cd59b	CD59b antigen
-2.33	Kcng4	potassium voltage-gated channel, subfamily G, member 4
-2.44	Cd59a	CD59a antigen
-2.63	Myoz1	myozenin 1
-2.78	Grb14	growth factor receptor bound protein 14
-2.86	Aldh1a1	aldehyde dehydrogenase family 1, subfamily A1
-2.86	Maob	monoamine oxidase B
-3.00	Gm1078	gene model 1078, (NCBI)
-3.13	Ppp1r1a	protein phosphatase 1, regulatory (inhibitor) subunit 1A
-3.85	Nos1	nitric oxide synthase 1, neuronal

Figure 10. Affymetrix array results of 3-mo-old soleus muscle. Changes in gene expression reflect the fiber type transition from fast twitch to slow twitch.

The reduced phosphorylation at serine 11878 could then reflect a compensatory mechanism to reduce the effects of the increased passive stress caused by additional differential splicing. However, considering that passive stress in IG KO mice is increased, this compensatory effect is apparently insufficient to counter the increased passive stress caused by the deletion of PEVK exons from the mutant titins in the IG KO mice.

Ankrd1 is not necessary for additional differential splicing of titin

Cardiac ankyrin repeat protein (*Ankrd1*), as its name implies, is found at high levels in cardiac muscle and is present at very low levels in skeletal muscles (Kojic et al., 2011). In IG KO mice, *Ankrd1* was found to be significantly induced both at the level of mRNA (Affymetrix microarray) and protein (Western blot). The role of *Ankrd1* in differential splicing of titin warranted investigation as deletion of *Ankrd1* in conjunction with removal of family members *Ankrd2* and *Ankrd3* (DARP/MARP3; MKO) causes in skeletal muscle an increase in titin size (Barash et al., 2007). *Ankrd1* also is an obvious candidate as it can signal from the sarcomere, where it binds titin, and translocate to the nucleus, where it can act as a transcription factor to regulate gene expression (Miller et al., 2003; Witt et al., 2004). To test whether *Ankrd1* was necessary for additional differential splicing, we created an IG, *Ankrd1* double KO. Soleus muscle from mice deficient in both *Ankrd1* and proximal Ig domains (IG KO, *Ankrd1* KO) express two mutant titin isoforms just as in IG KO mice, indicating that *Ankrd1* is not necessary for the additional differential splicing of titin. We cannot rule out the possibility that redundancy in function of the other *Ankrd1* family members, *Ankrd2* and *Ankrd3*, to compensate and allow splicing but have shown that *Ankrd1* on its own is not necessary for the additional differential splicing of titin.

It was previously hypothesized by Laure et al. (2009) that *Ankrd1* plays a role in the fiber type switching to fast-twitch fibers as *Ankrd* is consistently up-regulated in models of muscular dystrophy, including mice deficient for calpain 3, dysferlin, α-sarcoglycan, and dystrophin. The IG KO mouse model is unique from the muscular dystrophy models in that a shift toward slow-twitch fibers is observed in the soleus muscle. As expected by a shift in isoform composition to expression of slower MHC, soleus muscle from IG KO mice had a change in mRNA transcript expression that reflects a change in fiber type composition to slower and a resistance to fatigue as measured by intact muscle mechanics. This finding indicates that *Ankrd1* is not responsible for the fiber type switching to fast fibers, as the IG KO mouse has *Ankrd1* up-regulation and a switch toward slow fiber type. Our Affymetrix microarray data support the notion that the calcineurin–NFAT pathway is regulating the fiber type transition through the down-regulation of myozenin-1 (also known

as calsarcin-2, Fatz-1). Mice deficient in this protein have an increase in calcineurin activity and a fiber type switch to type 1 fibers (Frey et al., 2004).

Ankrd1 also has been previously shown to act as a transcription factor in the nucleus to alter gene expression through inhibition of the NF-κB pathway (Laure et al., 2010). Signaling through NF-κB affects numerous cell functions, including survival, proliferation, inflammation, and apoptosis (Peterson and Guttridge, 2008). Our Affymetrix microarray results are inconsistent with inhibition of the NF-κB pathway by *Ankrd1*. Although NOS-1 is down-regulated as expected (Peterson and Guttridge, 2008), Nrcam (Simpson and Morris, 2000) and UCP-2 (Lee et al., 1999), which are transcriptionally activated by NF-κB, are up-regulated. These previous studies were performed in human neuroblastoma SK-N-SH cells, neurons, and hepatocytes, respectively, and NF-κB signaling may regulate these genes differently in skeletal muscle. These findings show that although *Ankrd1* is up-regulated in muscle lysates, it is unlikely inhibiting the NF-κB pathway to regulate gene expression.

RBM20 expression regulates differential splicing of titin

RBM20 is a splicing factor that has been recently shown to affect titin splicing. RBM20 contains a centrally located RRM that provides RNA binding specificity and a C-terminal RS domain (rich in arginine and serine) that promotes protein–protein interactions and recruits RBM20 to the spliceosome (Guo et al., 2012; Li et al., 2013). In an in vitro splice reporter assay, RBM20 levels affect the inclusion of PEVK exons (Guo et al., 2012; Li et al., 2013). Levels of RBM20 protein expression have been previously found to correlate with the changes in titin size that occur during development, and loss of RBM20 prevents developmentally regulated differential splicing from taking place (Guo et al., 2012; Li et al., 2013). In support of RBM20 being a candidate to affect differential splicing of titin, our titin exon microarray revealed that additional differential splicing occurred in the PEVK region of titin. In IG KO soleus muscle at 3 mo of age, RBM20 protein expression was up-regulated 2.1-fold (Fig. 9, A–C). The up-regulation of RBM20 is consistent with the prediction that more RBM20 leads to more splicing of titin and that RBM20 acts to splice in the PEVK region of titin mRNA.

To test more directly whether the increased expression of RBM20 protein is required for additional differential splicing to take place, we used a novel mouse model in which the RRM of RBM20 was deleted (RBM20$^{\Delta RRM}$). This model was made to only abolish the RNA-binding function of RBM20 and not alter the other functional domains within RBM20. Mice with a single copy or two copies of RBM20$^{\Delta RRM}$ display larger titin isoforms than that of WT mice. This data supports the idea that RBM20 regulates splicing in a concentration-dependent manner and that RBM20 is a central player in differential

splicing of titin mRNA. Importantly, titin in soleus muscle from IG KO mice that were also heterozygous for RBM20$^{\Delta RRM}$ (IG KO, RBM20$^{\Delta RRM}$ HET) was present as a single isoform only and was similar in size to WT titin. Thus, RBM20 protein level can modulate not only the size of the titin isoform, but also the number of isoforms expressed (two isoforms in IG KO and one isoform in WT). RBM20 protein expression might provide a possible therapeutic avenue to modulate titin size and alter titin-based passive stress.

Relevance to skeletal muscle disease

The deletion of proximal Ig domains in skeletal muscle titin is not known to naturally occur, but in disease states in which passive stress is increased, pathways similar to those occurring in the IG KO could be activated. One characterized example is facioscapulohumeral muscular dystrophy, which is the third most common muscular dystrophy after the dystrophinopathies and myotonic dystrophy and is associated with a typical pattern of muscle weakness (Richards et al., 2012). Single fibers from patient biopsies show a significant increase in titin-based passive stress (Lassche et al., 2013). The increase in passive stress might be caused by the expression of a shorter, stiffer titin molecule by modulation of RBM20 expression. There are also several characterized examples of increased muscle stiffness occurring in acquired skeletal muscle disorders. Among these patients with spasticity are cerebral palsy (Fridén and Lieber, 2003) and spinal cord injury patients (Olsson et al., 2006,) as well as acquired neuromyotonia (Vincent, 2008). Patients with these acquired skeletal muscle diseases could potentially benefit from alterations in titin-based passive stress to revert the increase stiffness observed. Additionally, chronic obstructive pulmonary disorder (COPD) is a well-studied example of reduced passive stress as a result of acquired skeletal muscle disease. COPD is characterized by a limitation of airflow that leads to inspiratory muscle dysfunction (Moore et al., 2006). The diaphragm muscle from patients with COPD shows a decrease in passive stress as compared with controls that results from an increase in titin size, specifically in the PEVK region of titin (Moore et al., 2006; Ottenheijm et al., 2006). In this case, modulation of titin-based passive stress to produce a longer and more-compliant titin isoform has occurred. It is intriguing to speculate that by manipulating RBM20 expression levels, titin size and passive stress could be normalized in the diaphragm of patients with COPD.

Titin plays an important role in passive and active skeletal muscle contractility (Muhle-Goll et al., 2001) and contributes to muscle weakness in titin-associated skeletal muscle diseases (Granzier and Labeit, 2005). The mechanism by which RBM20 protein is up-regulated to cause additional differential splicing in the IG KO soleus muscle merits further investigation. The IG KO model provides a valuable model to understand the

regulation of differential splicing that ultimately leads to changes titin isoform size and alterations of titin-based passive stress in the sarcomere.

REFERENCES

Agbulut, O., P. Noirez, F. Beaumont, and G. Butler-Browne. 2003. Myosin heavy chain isoforms in postnatal muscle development of mice. *Biol. Cell.* 95:399–406. http://dx.doi.org/10.1016/S0248-4900(03)00087-X

Bang, M.L., T. Centner, F. Fornoff, A.J. Geach, M. Gotthardt, M. McNabb, C.C. Witt, D. Labeit, C.C. Gregorio, H. Granzier, and S. Labeit. 2001. The complete gene sequence of titin, expression of an unusual approximately 700-kDa titin isoform, and its interaction with obscurin identify a novel Z-line to I-band linking system. *Circ. Res.* 89:1065–1072. http://dx.doi.org/10.1161/hh2301.100981

Barash, I.A., M.L. Bang, L. Mathew, M.L. Greaser, J. Chen, and R.L. Lieber. 2007. Structural and regulatory roles of muscle ankyrin repeat protein family in skeletal muscle. *Am. J. Physiol. Cell Physiol.* 293:C218–C227. http://dx.doi.org/10.1152/ajpcell.00055.2007

Buck, D., B.D. Hudson, C.A. Ottenheijm, S. Labeit, and H. Granzier. 2010. Differential splicing of the large sarcomeric protein nebulin during skeletal muscle development. *J. Struct. Biol.* 170:325–333. http://dx.doi.org/10.1016/j.jsb.2010.02.014

Chemello, F., C. Bean, P. Cancellara, P. Laveder, C. Reggiani, and G. Lanfranchi. 2011. Microgenomic analysis in skeletal muscle: expression signatures of individual fast and slow myofibers. *PLoS ONE.* 6:e16807. http://dx.doi.org/10.1371/journal.pone.0016807

Chung, C.S., K.R. Hutchinson, M. Methawasin, C. Saripalli, J.E. Smith III, C.G. Hidalgo, X. Luo, S. Labeit, C. Guo, and H.L. Granzier. 2013. Shortening of the elastic tandem immunoglobulin segment of titin leads to diastolic dysfunction. *Circulation.* 128:19–28. http://dx.doi.org/10.1161/CIRCULATIONAHA.112.001268

Coulis, G., S. Becila, C.H. Herrera-Mendez, M.A. Sentandreu, F. Raynaud, I. Richard, Y. Benyamin, and A. Ouali. 2008. Calpain 1 binding capacities of the N1-line region of titin are significantly enhanced by physiological concentrations of calcium. *Biochemistry.* 47:9174–9183. http://dx.doi.org/10.1021/bi800315v

Frey, N., T. Barrientos, J.M. Shelton, D. Frank, H. Rütten, D. Gehring, C. Kuhn, M. Lutz, B. Rothermel, R. Bassel-Duby, et al. 2004. Mice lacking calsarcin-1 are sensitized to calcineurin signaling and show accelerated cardiomyopathy in response to pathological biomechanical stress. *Nat. Med.* 10:1336–1343. http://dx.doi.org/10.1038/nm1132

Fridén, J., and R.L. Lieber. 2003. Spastic muscle cells are shorter and stiffer than normal cells. *Muscle Nerve.* 27:157–164. http://dx.doi.org/10.1002/mus.10247

Friedman, A.D. 2009. Cell cycle and developmental control of hematopoiesis by Runx1. *J. Cell. Physiol.* 219:520–524. http://dx.doi.org/10.1002/jcp.21738

Fukuda, N., and H.L. Granzier. 2005. Titin/connectin-based modulation of the Frank-Starling mechanism of the heart. *J. Muscle Res. Cell Motil.* 26:319–323. http://dx.doi.org/10.1007/s10974-005-9038-1

Fukuda, N., H.L. Granzier, S. Ishiwata, and S. Kurihara. 2008. Physiological functions of the giant elastic protein titin in mammalian striated muscle. *J. Physiol. Sci.* 58:151–159. http://dx.doi.org/10.2170/physiolsci.RV005408

Fürst, D.O., M. Osborn, R. Nave, and K. Weber. 1988. The organization of titin filaments in the half-sarcomere revealed by monoclonal antibodies in immunoelectron microscopy: a map of ten nonrepetitive epitopes starting at the Z line extends close to the M line. *J. Cell Biol.* 106:1563–1572. http://dx.doi.org/10.1083/jcb.106.5.1563

Gautel, M. 2011. The sarcomeric cytoskeleton: who picks up the strain? *Curr. Opin. Cell Biol.* 23:39–46. http://dx.doi.org/10.1016/j.ceb.2010.12.001

Granzier, H.L., and T.C. Irving. 1995. Passive tension in cardiac muscle: contribution of collagen, titin, microtubules, and intermediate filaments. *Biophys. J.* 68:1027–1044. http://dx.doi.org/10.1016/S0006-3495(95)80278-X

Granzier, H.L., and S. Labeit. 2005. Titin and its associated proteins: the third myofilament system of the sarcomere. *Adv. Protein Chem.* 71:89–119. http://dx.doi.org/10.1016/S0065-3233(04)71003-7

Granzier, H., and S. Labeit. 2007. Structure-function relations of the giant elastic protein titin in striated and smooth muscle cells. *Muscle Nerve.* 36:740–755. http://dx.doi.org/10.1002/mus.20886

Granzier, H.L., M.H. Radke, J. Peng, D. Westermann, O.L. Nelson, K. Rost, N.M. King, Q. Yu, C. Tschöpe, M. McNabb, et al. 2009. Truncation of titin's elastic PEVK region leads to cardiomyopathy with diastolic dysfunction. *Circ. Res.* 105:557–564. http://dx.doi.org/10.1161/CIRCRESAHA.109.200964

Greaser, M.L., S.M. Wang, M. Berri, P. Mozdziak, and Y. Kumazawa. 2000. Sequence and mechanical implications of titin's PEVK region. *Adv. Exp. Med. Biol.* 481:53–66. http://dx.doi.org/10.1007/978-1-4615-4267-4_4

Greer, K.A., M.R. McReynolds, H.L. Brooks, and J.B. Hoying. 2006. CARMA: A platform for analyzing microarray datasets that incorporate replicate measures. *BMC Bioinformatics.* 7:149. http://dx.doi.org/10.1186/1471-2105-7-149

Grozdanovic, Z., and H.G. Baumgarten. 1999. Nitric oxide synthase in skeletal muscle fibers: a signaling component of the dystrophin-glycoprotein complex. *Histol. Histopathol.* 14:243–256.

Guo, W., S. Schafer, M.L. Greaser, M.H. Radke, M. Liss, T. Govindarajan, H. Maatz, H. Schulz, S. Li, A.M. Parrish, et al. 2012. RBM20, a gene for hereditary cardiomyopathy, regulates titin splicing. *Nat. Med.* 18:766–773. http://dx.doi.org/10.1038/nm.2693

Hayashi, C., Y. Ono, N. Doi, F. Kitamura, M. Tagami, R. Mineki, T. Arai, H. Taguchi, M. Yanagida, S. Hirner, et al. 2008. Multiple molecular interactions implicate the connectin/titin N2A region as a modulating scaffold for p94/calpain 3 activity in skeletal muscle. *J. Biol. Chem.* 283:14801–14814. http://dx.doi.org/10.1074/jbc.M708262200

Hidalgo, C., and H. Granzier. 2013. Tuning the molecular giant titin through phosphorylation: role in health and disease. *Trends Cardiovasc. Med.* 23:165–171. http://dx.doi.org/10.1016/j.tcm.2012.10.005

Hidalgo, C., B. Hudson, J. Bogomolovas, Y. Zhu, B. Anderson, M. Greaser, S. Labeit, and H. Granzier. 2009. PKC phosphorylation of titin's PEVK element: a novel and conserved pathway for modulating myocardial stiffness. *Circ. Res.* 105:631–638: 17: 638. http://dx.doi.org/10.1161/CIRCRESAHA.109.198465

Horowits, R., and R.J. Podolsky. 1987. The positional stability of thick filaments in activated skeletal muscle depends on sarcomere length: evidence for the role of titin filaments. *J. Cell Biol.* 105: 2217–2223. http://dx.doi.org/10.1083/jcb.105.5.2217

Hudson, B.D., C.G. Hidalgo, M. Gotthardt, and H.L. Granzier. 2010. Excision of titin's cardiac PEVK spring element abolishes PKCalpha-induced increases in myocardial stiffness. *J. Mol. Cell. Cardiol.* 48:972–978. http://dx.doi.org/10.1016/j.yjmcc.2009.12.006

Kojic, S., D. Radojkovic, and G. Faulkner. 2011. Muscle ankyrin repeat proteins: their role in striated muscle function in health and disease. *Crit. Rev. Clin. Lab. Sci.* 48:269–294. http://dx.doi.org/10.3109/10408363.2011.643857

Labeit, S., and B. Kolmerer. 1995. Titins: giant proteins in charge of muscle ultrastructure and elasticity. *Science.* 270:293–296. http://dx.doi.org/10.1126/science.270.5234.293

Labeit, D., K. Watanabe, C. Witt, H. Fujita, Y. Wu, S. Lahmers, T. Funck, S. Labeit, and H. Granzier. 2003. Calcium-dependent molecular spring elements in the giant protein titin. *Proc. Natl. Acad. Sci. USA.* 100:13716–13721. http://dx.doi.org/10.1073/pnas.2235652100

Labeit, S., C.H. Kohl, C.C. Witt, D. Labeit, J. Jung, and H. Granzier. 2010. Modulation of muscle atrophy, fatigue and MLC phosphorylation by MuRF1 as indicated by hindlimb suspension studies on MuRF1-KO mice. *J. Biomed. Biotechnol.* 2010:693741. http://dx.doi.org/10.1155/2010/693741

Lahmers, S., Y. Wu, D.R. Call, S. Labeit, and H. Granzier. 2004. Developmental control of titin isoform expression and passive stiffness in fetal and neonatal myocardium. *Circ. Res.* 94:505–513. http://dx.doi.org/10.1161/01.RES.0000115522.52554.86

Lassche, S., G.J. Stienen, T.C. Irving, S.M. van der Maarel, N.C. Voermans, G.W. Padberg, H. Granzier, B.G. van Engelen, and C.A. Ottenheijm. 2013. Sarcomeric dysfunction contributes to muscle weakness in facioscapulohumeral muscular dystrophy. *Neurology.* 80:733–737. http://dx.doi.org/10.1212/WNL.0b013e318282513b

Laure, L., L. Suel, C. Roudaut, N. Bourg, A. Ouali, M. Bartoli, I. Richard, and N. Danièle. 2009. Cardiac ankyrin repeat protein is a marker of skeletal muscle pathological remodelling. *FEBS J.* 276:669–684. http://dx.doi.org/10.1111/j.1742-4658.2008.06814.x

Laure, L., N. Danièle, L. Suel, S. Marchand, S. Aubert, N. Bourg, C. Roudaut, S. Duguez, M. Bartoli, and I. Richard. 2010. A new pathway encompassing calpain 3 and its newly identified substrate cardiac ankyrin repeat protein is involved in the regulation of the nuclear factor-κB pathway in skeletal muscle. *FEBS J.* 277:4322–4337. http://dx.doi.org/10.1111/j.1742-4658.2010.07820.x

Laws, N., and A. Hoey. 2004. Progression of kyphosis in mdx mice. *J. Appl. Physiol.* 97:1970–1977. http://dx.doi.org/10.1152/japplphysiol.01357.2003

Lee, F.Y., Y. Li, H. Zhu, S. Yang, H.Z. Lin, M. Trush, and A.M. Diehl. 1999. Tumor necrosis factor increases mitochondrial oxidant production and induces expression of uncoupling protein-2 in the regenerating mice [correction of rat] liver. *Hepatology.* 29:677–687. http://dx.doi.org/10.1002/hep.510290320

LeWinter, M.M., and H. Granzier. 2010. Cardiac titin: a multifunctional giant. *Circulation.* 121:2137–2145. http://dx.doi.org/10.1161/CIRCULATIONAHA.109.860171

Li, S., W. Guo, C.N. Dewey, and M.L. Greaser. 2013. Rbm20 regulates titin alternative splicing as a splicing repressor. *Nucleic Acids Res.* 41:2659–2672. http://dx.doi.org/10.1093/nar/gks1362

Linke, W.A., and M. Krüger. 2010. The giant protein titin as an integrator of myocyte signaling pathways. *Physiology (Bethesda).* 25:186–198. http://dx.doi.org/10.1152/physiol.00005.2010

Linke, W.A., V.I. Popov, and G.H. Pollack. 1994. Passive and active tension in single cardiac myofibrils. *Biophys. J.* 67:782–792. http://dx.doi.org/10.1016/S0006-3495(94)80538-7

Miller, M.K., M.L. Bang, C.C. Witt, D. Labeit, C. Trombitas, K. Watanabe, H. Granzier, A.S. McElhinny, C.C. Gregorio, and S. Labeit. 2003. The muscle ankyrin repeat proteins: CARP, ankrd2/Arpp and DARP as a family of titin filament-based stress response molecules. *J. Mol. Biol.* 333:951–964. http://dx.doi.org/10.1016/j.jmb.2003.09.012

Moore, A.J., A. Stubbings, E.B. Swallow, M. Dusmet, P. Goldstraw, R. Porcher, J. Moxham, M.I. Polkey, and M.A. Ferenczi. 2006. Passive properties of the diaphragm in COPD. *J. Appl. Physiol.* 101:1400–1405. http://dx.doi.org/10.1152/japplphysiol.01614.2005

Muhle-Goll, C., M. Habeck, O. Cazorla, M. Nilges, S. Labeit, and H. Granzier. 2001. Structural and functional studies of titin's fn3 modules reveal conserved surface patterns and binding to myosin S1—a possible role in the Frank-Starling mechanism of the heart. *J. Mol. Biol.* 313:431–447. http://dx.doi.org/10.1006/jmbi.2001.5017

Olsson, M.C., M. Krüger, L.H. Meyer, L. Ahnlund, L. Gransberg, W.A. Linke, and L. Larsson. 2006. Fibre type-specific increase in passive muscle tension in spinal cord-injured subjects with spasticity. *J. Physiol.* 577:339–352. http://dx.doi.org/10.1113/jphysiol.2006.116749

Ottenheijm, C.A., and H. Granzier. 2010. Role of titin in skeletal muscle function and disease. *Adv. Exp. Med. Biol.* 682:105–122. http://dx.doi.org/10.1007/978-1-4419-6366-6_6

Ottenheijm, C.A., L.M. Heunks, T. Hafmans, P.F. van der Ven, C. Benoist, H. Zhou, S. Labeit, H.L. Granzier, and P.N. Dekhuijzen. 2006. Titin and diaphragm dysfunction in chronic obstructive pulmonary disease. *Am. J. Respir. Crit. Care Med.* 173:527–534. http://dx.doi.org/10.1164/rccm.200507-1056OC

Ottenheijm, C.A., C. Hidalgo, K. Rost, M. Gotthardt, and H. Granzier. 2009a. Altered contractility of skeletal muscle in mice deficient in titin's M-band region. *J. Mol. Biol.* 393:10–26. http://dx.doi.org/10.1016/j.jmb.2009.08.009

Ottenheijm, C.A., A.M. Knottnerus, D. Buck, X. Luo, K. Greer, A. Hoying, S. Labeit, and H. Granzier. 2009b. Tuning passive mechanics through differential splicing of titin during skeletal muscle development. *Biophys. J.* 97:2277–2286. http://dx.doi.org/10.1016/j.bpj.2009.07.041

Ottenheijm, C.A., N.C. Voermans, B.D. Hudson, T. Irving, G.J. Stienen, B.G. van Engelen, and H. Granzier. 2012. Titin-based stiffening of muscle fibers in Ehlers-Danlos Syndrome. *J. Appl. Physiol.* 112: 1157–1165. http://dx.doi.org/10.1152/japplphysiol.01166.2011

Peterson, J.M., and D.C. Guttridge. 2008. Skeletal muscle diseases, inflammation, and NF-kappaB signaling: insights and opportunities for therapeutic intervention. *Int. Rev. Immunol.* 27:375–387. http://dx.doi.org/10.1080/08830180802302389

Pfuhl, M., and A. Pastore. 1995. Tertiary structure of an immunoglobulin-like domain from the giant muscle protein titin: a new member of the I set. *Structure.* 3:391–401. http://dx.doi.org/10.1016/S0969-2126(01)00170-8

Prado, L.G., I. Makarenko, C. Andresen, M. Krüger, C.A. Opitz, and W.A. Linke. 2005. Isoform diversity of giant proteins in relation to passive and active contractile properties of rabbit skeletal muscles. *J. Gen. Physiol.* 126:461–480. http://dx.doi.org/10.1085/jgp.200509364

Radke, M.H., J. Peng, Y. Wu, M. McNabb, O.L. Nelson, H. Granzier, and M. Gotthardt. 2007. Targeted deletion of titin N2B region leads to diastolic dysfunction and cardiac atrophy. *Proc. Natl. Acad. Sci. USA.* 104:3444–3449. http://dx.doi.org/10.1073/pnas.0608543104

Richards, M., F. Coppée, N. Thomas, A. Belayew, and M. Upadhyaya. 2012. Facioscapulohumeral muscular dystrophy (FSHD): an enigma unravelled? *Hum. Genet.* 131:325–340. http://dx.doi.org/10.1007/s00439-011-1100-z

Rivero, J.L., R.J. Talmadge, and V.R. Edgerton. 1998. Fibre size and metabolic properties of myosin heavy chain-based fibre types in

rat skeletal muscle. *J. Muscle Res. Cell Motil.* 19:733–742. http://dx.doi.org/10.1023/A:1005482816442

Saido, T.C., S. Nagao, M. Shiramine, M. Tsukaguchi, H. Sorimachi, H. Murofushi, T. Tsuchiya, H. Ito, and K. Suzuki. 1992. Autolytic transition of mu-calpain upon activation as resolved by antibodies distinguishing between the pre- and post-autolysis forms. *J. Biochem.* 111:81–86.

Simpson, C.S., and B.J. Morris. 2000. Regulation of neuronal cell adhesion molecule expression by NF-kappa B. *J. Biol. Chem.* 275:16879–16884. http://dx.doi.org/10.1074/jbc.275.22.16879

Sorimachi, H., S. Hata, and Y. Ono. 2011. Impact of genetic insights into calpain biology. *J. Biochem.* 150:23–37. http://dx.doi.org/10.1093/jb/mvr070

Trombitás, K., M. Greaser, G. French, and H. Granzier. 1998. PEVK extension of human soleus muscle titin revealed by immunolabeling with the anti-titin antibody 9D10. *J. Struct. Biol.* 122:188–196. http://dx.doi.org/10.1006/jsbi.1998.3984

Trombitás, K., Y. Wu, D. Labeit, S. Labeit, and H. Granzier. 2001. Cardiac titin isoforms are coexpressed in the half-sarcomere and extend independently. *Am. J. Physiol. Heart Circ. Physiol.* 281:H1793–H1799.

van Hees, H.W., C.A. Ottenheijm, H.L. Granzier, P.N. Dekhuijzen, and L.M. Heunks. 2010. Heart failure decreases passive tension generation of rat diaphragm fibers. *Int. J. Cardiol.* 141:275–283. http://dx.doi.org/10.1016/j.ijcard.2008.12.042

van Hees, H.W., W.J. Schellekens, G.L. Andrade Acuña, M. Linkels, T. Hafmans, C.A. Ottenheijm, H.L. Granzier, G.J. Scheffer, J.G. van der Hoeven, P.N. Dekhuijzen, and L.M. Heunks. 2012. Titin and diaphragm dysfunction in mechanically ventilated rats. *Intensive Care Med.* 38:702–709. http://dx.doi.org/10.1007/s00134-012-2504-5

Vincent, A. 2008. Autoimmune disorders of the neuromuscular junction. *Neurol. India.* 56:305–313. http://dx.doi.org/10.4103/0028-3886.43449

Warren, C.M., P.R. Krzesinski, and M.L. Greaser. 2003. Vertical agarose gel electrophoresis and electroblotting of high-molecular-weight proteins. *Electrophoresis.* 24:1695–1702. http://dx.doi.org/10.1002/elps.200305392

Watanabe, K., C. Muhle-Goll, M.S. Kellermayer, S. Labeit, and H. Granzier. 2002. Different molecular mechanics displayed by titin's constitutively and differentially expressed tandem Ig segments. *J. Struct. Biol.* 137:248–258. http://dx.doi.org/10.1006/jsbi.2002.4458

Witt, C.C., Y. Ono, E. Puschmann, M. McNabb, Y. Wu, M. Gotthardt, S.H. Witt, M. Haak, D. Labeit, C.C. Gregorio, et al. 2004. Induction and myofibrillar targeting of CARP, and suppression of the Nkx2.5 pathway in the MDM mouse with impaired titin-based signaling. *J. Mol. Biol.* 336:145–154. http://dx.doi.org/10.1016/j.jmb.2003.12.021

Wu, Y., S.P. Bell, K. Trombitas, C.C. Witt, S. Labeit, M.M. LeWinter, and H. Granzier. 2002. Changes in titin isoform expression in pacing-induced cardiac failure give rise to increased passive muscle stiffness. *Circulation.* 106:1384–1389. http://dx.doi.org/10.1161/01.CIR.0000029804.61510.02